Epitaxy-Assisted Creation of PCBM Nanocrystals and Its Application in Constructing Optimized Morphology for Bulk-Heterojunction Polymer Solar Cells

ARTICLE *in* THE JOURNAL OF PHYSICAL CHEMISTRY B · JANUARY 2009

Impact Factor: 3.3 · DOI: 10.1021/jp8081529 · Source: PubMed

5 AUTHORS, INCLUDING:

Ligui Li
South China University of Technology
56 PUBLICATIONS **915** CITATIONS
SEE PROFILE

Guanghao Lu
University of Massachusetts Amherst
24 PUBLICATIONS **650** CITATIONS
SEE PROFILE

Sijun Li
University of Antwerp
15 PUBLICATIONS **120** CITATIONS
SEE PROFILE

THE JOURNAL OF PHYSICAL CHEMISTRY B

Article

Epitaxy-Assisted Creation of PCBM Nanocrystals and Its Application in Constructing Optimized Morphology for Bulk-Heterojunction Polymer Solar Cells

Ligui Li, Guanghao Lu, Sijun Li, Haowei Tang, and Xiaoniu Yang

J. Phys. Chem. B, **2008**, 112 (49), 15651-15658• DOI: 10.1021/jp8081529 • Publication Date (Web): 12 November 2008

Epitaxy-Assisted Creation of PCBM Nanocrystals and Its Application in Constructing Optimized Morphology for Bulk-Heterojunction Polymer Solar Cells

Ligui Li, Guanghao Lu, Sijun Li, Haowei Tang, and Xiaoniu Yang*

State Key Laboratory of Polymer Physics and Chemistry, Changchun Institute of Applied Chemistry, Chinese Academy of Sciences, Graduate School of the Chinese Academy of Sciences, Changchun 130022, P. R. China

Received: September 13, 2008; Revised Manuscript Received: September 28, 2008

PCBM (a C_{60} derivative) is so far the most successful electron acceptor for bulk-heterojunction polymer photovoltaic (PV) cells. Here we present a novel method epitaxy-assisted creation of PCBM nanocrystals and their homogeneous distribution in the matrix using freshly cleaved mica sheet as the substrate. The highly matched epitaxy relationship between the unit cell of PCBM crystal and crystallographic (001) surface of mica induces abundant PCBM nuclei, which subsequently develop into nanoscale crystals with homogeneous dispersion in the composite film. Both the shape and size of these nanocrystals could be tuned via choosing the type of matrix polymer, film thickness, ratio of PCBM in the composite film, and annealing temperature. Thus, the obtained thin composite film is removed from the original mica substrate via the flotation technique and transferred to a real substrate for device completion. The success of this method has been verified by the substantially improved device performance, in particular the increased short-circuit current, which is heavily dependent on the morphology of the photoactive layer. Therefore, we have actually demonstrated a novel approach to construct preferred morphology for high-performance optoelectronic devices via resorting to other specific substrates which could induce the formation of this type morphology.

Introduction

The electron donor−acceptor approach serves as an crucial development for exciton splitting into free charge carriers so as to generate photovoltaic electricity in polymer solar cells, whose development has attracted more and more attention due to the advantages of low-cost, roll-to-roll production, mechanical flexibility, and large area by using the well-developed solution-based thin film deposition technology.[1−3] However, the exciton dissociation and charge carrier transportation in the thus-obtained donor−acceptor system is heavily influenced by the morphology of the components involved. Therefore, apart from the significance of introducing low band gap materials[4−6] to reduce the mismatched absorption of photoactive layer with incident solar spectrum, another key issue to fabricate high-performance polymer solar cells is to achieve an optimized morphology for photovoltaic layer.[7−18] Since the limited exciton diffusion in organic semiconductor, a large-scale phase separation in between the donor and acceptor components should be prevented. A few methods such as the types of solvent employed,[9] crystallizability of components involved,[19,20] spatial confinement during the treatment,[21] using aqueous solution with dispersed nanoparticles for thin film deposition,[22] and so on have been applied to reduce the scale of phase segregation during device fabrication, whereas another very important morphology requirement which also significantly influences the ultimate device performance, i.e. continuous pathways for both electrons and holes to be transported to the appropriate electrodes, is still a challenge. To satisfy this criterion, however, it requires to increase the length scale of phase segregation in the perpendicular direction, preferably continuous and straight pathways connecting directly to the corresponding electrodes for fast transport of holes and electrons,[23,24] eliminating the loss which resulted from recombination. The commonly adopted post-treatment methods, namely, thermal treatment[25] and solvent annealing,[26−28] have been proven to be effective in improving the device performance, but when applying such treatments, delicate attention should be paid since it is easy to cause large-scale phase segregation in the photoactive layer.[29] Therefore, the contradictory morphological requirements, namely the small-scale phase segregation to form large interfacial area for efficient exciton dissociation and the increased phase segregation so as to achieve more continuous and straight pathways for free charge carrier transport directly, make morphology control more complicated and difficult.

So far, the fullerene derivatives are still the most successful acceptor materials in the present polymer solar cells in terms of device performance[26,30−32] and of which the [6,6]-phenyl C_{61} butyric acid methyl ester (PCBM) is the most commonly used one due to its high solubility in common organic solvents. Otero et al.[33] have developed a new method by using chemical vapor deposition to achieve controllable morphology for the blends of small organic donor molecules with PCBM. However, to the best of our knowledge, there is almost no effective method to control the morphology of PCBM in the photoactive layer toward nanoscale (for instance, sub-50 nm) aggregates (crystals) so as to create short and continuous pathways for electron transport. The main reason is that although PCBM is a crystallizable molecule, it is very difficult to nucleate homogeneously within the whole film to form nanoscale crystals. Consequently, the composite film is either very homogeneous without obvious phase separation or PCBM crystallizes into crystals with several microns upon conventional thermal annealing, leading to large-scale phase separation in the film. Nevertheless, it is well documented that some novel structures can be well achieved by using the epitaxial method,[34−39] in which there is certain crystallographic *d*-spacing match between the ordered template and subsequently deposited layer. With the presence of ever-formed surface having specific lattice

* Corresponding author. E-mail: xnyang@ciac.jl.cn.

10.1021/jp8081529 CCC: $40.75
Published on Web 11/12/2008

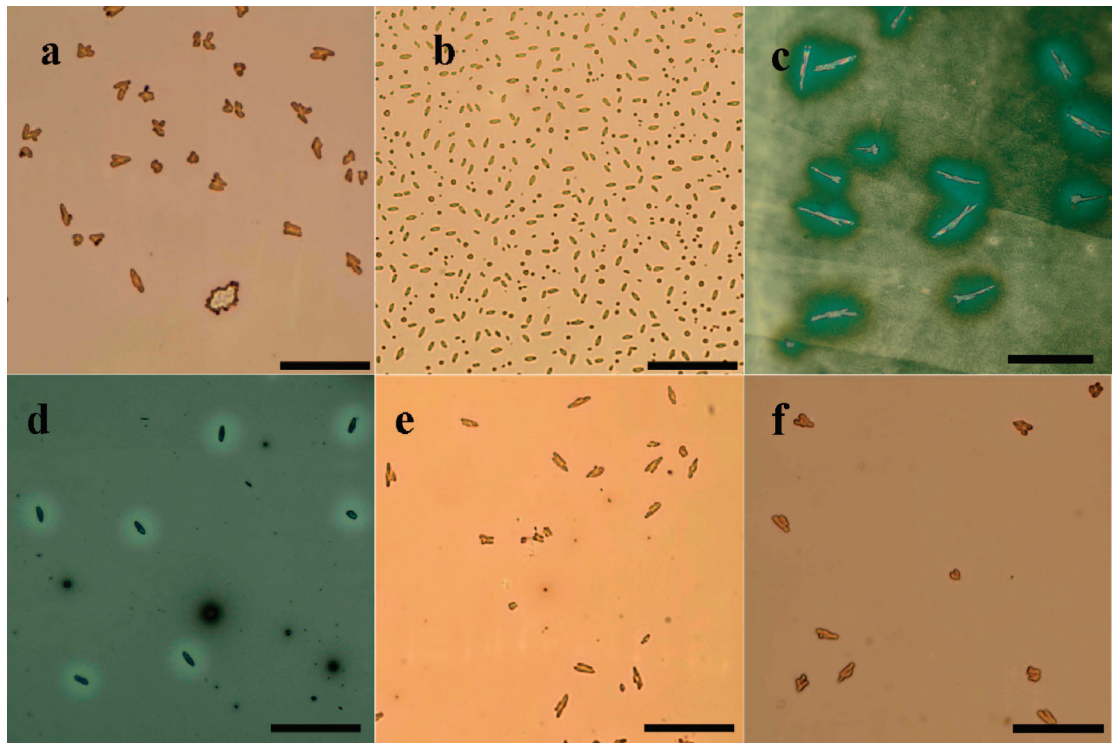

Figure 1. Typical morphology of P3HT:PCBM (1:1, w/w) composite films annealed at 150 °C for 30 min on different substrates: (a) glass, (b) freshly cleaved mica, (c) HOPG (001) plane, (d) silicon (100) plane, (e) quartz (001) plane, (f) PEDOT:PSS/mica. Scale bar: 50 μm.

spacing, the newly deposited material is easier to crystallize since it takes much less time for the nucleation process, which is usually the bottleneck step during the initial stage of crystallization. In such a case, epitaxial growth could result in the crystals with both large population and uniform size. In the present work, we first disclose the unique epitaxial relation between PCBM and the freshly cleaved mica substrate and then apply this finding to construct homogeneously and abundantly PCBM nanocrystals in its composite films with conjugated polymers. The feasibility and success of this novel method are eventually verified by the real device fabrication and thus-obtained device with substantially improved performance, respectively.

Experimental Section

Materials. Poly(3-hexylthiophene) (P3HT) with M_w = 100 000 g mol^{-1} and regioregularity better than 98% was purchased from Rieke Metals Inc. PCBM and *o*-dichlorobenzene (ODCB, anhydrous, 99%) were purchased from Sigma-Aldrich Co. Ltd. MDMO-PPV with M_w = 1 000 000 g mol^{-1} was obtained from Philips Research Eindhoven. All these materials were used as received without further treatment.

Sample Preparations. The P3HT:PCBM (1:1, w/w) and MDMO-PPV:PCBM (1:2, w/w) solutions were prepared by putting a certain amount of materials in *o*-dichlorobenzene (ODCB) solvent to achieve the solutions with conjugated polymer concentration of 8.0 and 4.0 mg mL^{-1}, respectively. These mixtures were stirred in the dark overnight under nitrogen protection.

The thin films were obtained via spin-coating (Laurell Spin Processor WS-400B 6NPP Lite) the as-prepared solutions onto precleaned substrates, i.e. glass, silicon, PEDOT:PSS/mica, quartz, freshly cleaved highly oriented pyrolytic graphite (HOPG), and freshly cleaved mica sheets. The PEDOT:PSS/mica substrate was first prepared by spin-coating aqueous PEDOT:PSS solution onto the mica sheets and then dried on hot plate at 80 °C for 5 h in a vacuum.

For the device fabrication, the pristine composite films were first deposited on mica substrate. The homogenously distributed PCBM nanocrystals in the composite films were constructed upon thermal annealing in an inert atmosphere. Afterward, the floatation technique was used to separate the P3HT:PCBM composite films from mica substrates on deionized water, and the films were subsequently transferred to real device substrate glass/ITO/PEDOT:PSS with an additionally very thin (~20 nm) layer of the same P3HT:PCBM (1:1, w/w) to prevent the PEDOT:PSS layer from being dissolved during film fishing. Finally, after the films had been dried in vacuum at room temperature, the devices were completed by evaporation of a 1 nm LiF layer and subsequently 100 nm Al back electrode.

Characterizations. Optical microscopy (OM) observations were carried out by using a Zeiss A1m optical microscope. Transmission electron microscopy (TEM) was performed on a JEOL JEM-1011 transmission electron microscope operated at an acceleration voltage of 100 kV. Surface topography was observed by atomic force microscopy (AFM) operating in tapping mode on SPA300HV with a SPI3800N controller (Seiko Instruments Inc., Japan) at room temperature. UV−vis absorption spectra were acquired on a Lambda 750 spectrometer (Perkin-Elmer, Wellesley, MA).

The performance characterization for the PV cells was carried out with a Keithley-2400 source meter. The cells are illuminated by a tungsten−halogen lamp (filtered by a Schott KG1 and GG385 filter resulting in a spectral range of 400−900 nm with a maximum at 650 nm) at an intensity of 100 mW/cm^2.

Results and Discussion

Figure 1 shows the typical morphology of P3HT:PCBM (1:1, w/w) composite films subjected to thermal annealing at 150 °C for 30 min on different substrates. After comparing thus-

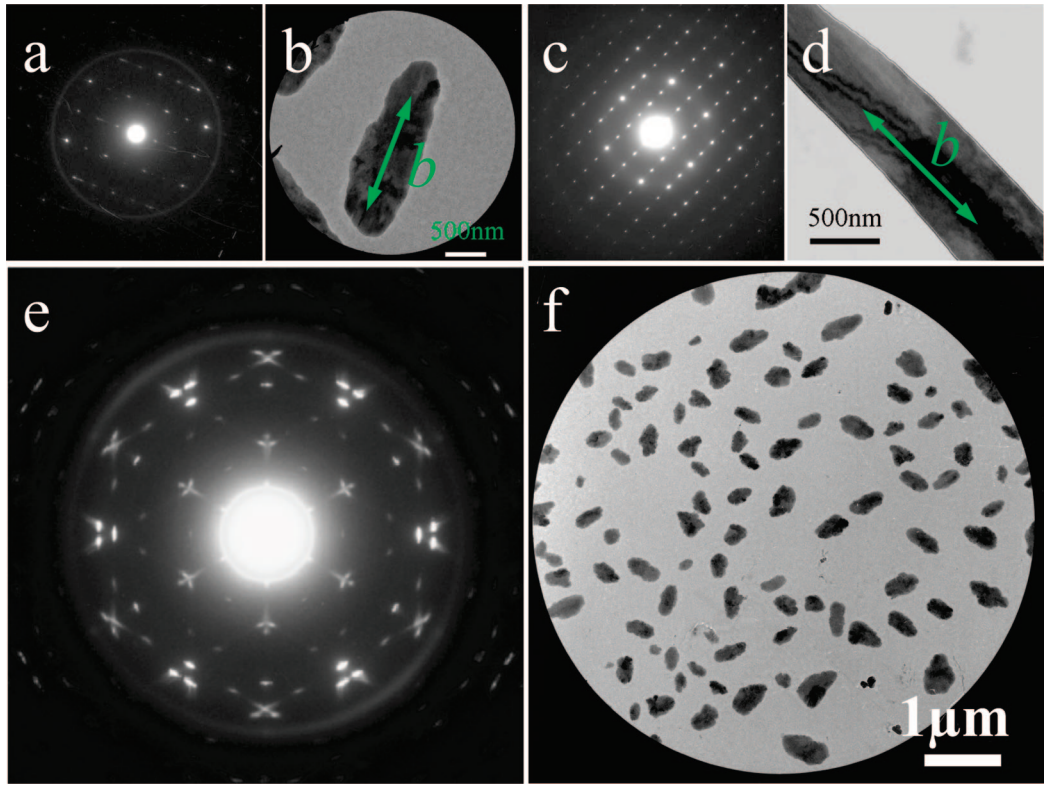

Figure 2. TEM images and their corresponding SAED patterns of PCBM crystals in P3HT:PCBM (1:1, w/w) (a, b, e, f) and MDMO-PPV:PCBM (1:2, w/w) (c, d) composite films after annealing at 150 °C for 30 min on mica substrate, respectively. (a), (c), and (e) are the corresponding SAED patterns of (b), (d), and (f), respectively.

obtained morphology of the composite films, tremendous morphology variation is observed between the composite film on freshly cleaved mica sheet and those on the other substrates. As revealed in Figure 1b, numerous ricelike PCBM crystals homogeneously distribute over the whole film investigated. In contrast, for the films on glass substrate, HOPG (001), silicon (100), and quartz (001) lattice surfaces, less but much larger and shapeless PCBM crystals are observed (Figure 1, parts a, c, d, and e, respectively). However, if this naked mica surface is decorated with a thin (ca. 50 nm) PEDOT:PSS layer and used as a substrate, the unique morphology observed on the naked mica substrate disappears, and only morphology similar to those observed in the other substrates is obtained (Figure 1f). On the basis of these observations, we speculate there is certain relationship between PCBM molecules and freshly cleaved mica substrate, which eventually contributes to the unique morphology obtained after thermal annealing in contrast to the other substrates.

To investigate this interesting PCBM crystallization on mica surface, we resorted to TEM study. As shown in Figure 2a, when performing SAED analysis on the ricelike PCBM domains in P3HT:PCBM (1:1, w/w) composite film after annealing on mica surface, a clear single crystal diffraction pattern is obtained,[40,41] indicating that these ricelike black domains are PCBM single crystals. Although the complete unit cell of PCBM crystal is still not fully clear, we could assume the obtained diffraction on the $a-b$ plane with c axis paralleling to the incident electron beam using previously obtained results.[41−44] By comparing the bright-field image in Figure 2b with its corresponding SAED pattern in Figure 2a, we presume that the crystallography b axis is the preferred growth direction of PCBM crystals. Thus, an incomplete unit cell with $a = 1.550$ nm, $b = 1.007$ nm, and $\gamma = 90°$ of PCBM crystal is obtained. After checking many SAED patterns with their corresponding bright-field image within the selected area (data not shown here), we observe that all the PCBM crystals have the same preferred growth direction. For comparison, the crystal growth behavior of PCBM in the MDMO-PPV:PCBM (1:2, w/w) composite film was also investigated. The same preferred growth direction along b axis and identical unit cell parameters were also observed (Figure 2c,d). When a much larger area (Figure 2f) was selected by increasing the diameter of field limiting aperture, which has included more than 100 PCBM crystals to contribute to the diffraction pattern, well-regulated diffraction spots as shown in Figure 2e instead of typical diffraction rings were observed, implying the orientations of these PCBM crystals are confined to a few specific directions.

By using the suggested unit cell of PCBM crystals as mentioned above, i.e. $a = 1.550$ nm, $b = 1.007$ nm, and $\gamma = 90°$, it is found that this diffraction pattern could be indexed by a 3-fold superposition of PCBM single crystals, indicating all the crystals within this selected area could be classified into three groups according to their unique orientations. The detailed indexes to this diffraction pattern are shown in Figure 3a, in which each color (i.e., red, green, and blue) stands for the diffraction spots contributed by a group of PCBM crystals, which has been stained in corresponding color as shown in Figure 3b. Therefore, both the diffraction pattern and bright-field micrograph have clearly demonstrated that the orientation of the PCBM crystals within a group forms an angle of 60° or −60° with the crystals in the other groups.

To further verify our observation, we performed quantitative analysis on these morphological data. As shown in Figure 4a, it shows rodlike PCBM crystals are homogeneously dispersed in the MDMO-PPV:PCBM (1:2, w/w) composite film after thermal annealing. However, upon performing a fast Fourier transfer (FFT) on this micrograph, as given in the inset, a pattern with hexagonal symmetry is obtained, which reveals that the

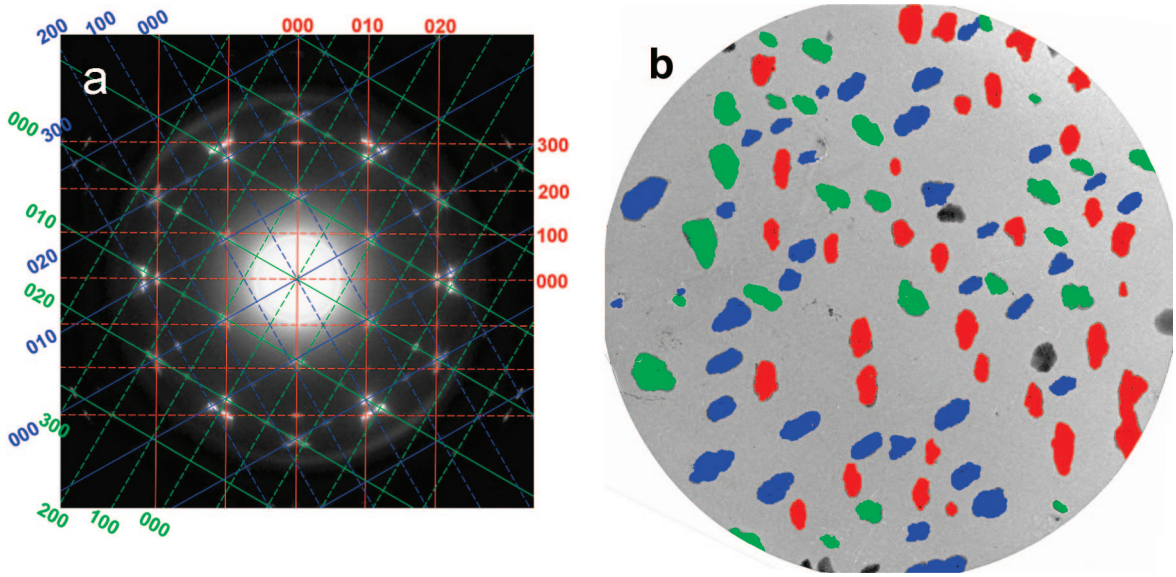

Figure 3. Detailed indexes of the SAED pattern contributed from the selected area of PCBM crystals, which have been marked with corresponding color red, green, and blue according to their different orientations. The original figures of parts a and b are Figures 2e and 2f, respectively.

preferred growth direction (orientation) of these rodlike crystals form an angle of −60° or 60° with that of the others. More specifically, the six outer diffraction spots are attributed to nearly the same diameter of these crystals. However, the appearance of seriously elongated spots in the inner part implies that the length of these rodlike crystals has somehow broad distribution. With respect to the P3HT:PCBM (1:1, w/w) composite (Figure 4b) prepared on mica, except the length of the crystals is shorter compared to that in the MDMO-PPV composite, a similar phenomenon is observed, which again confirms that the PCBM crystals grow on the freshly cleaved mica surface only take three preferred growth directions with the angle of 60° or −60° between each other. In contrast, as shown in Figure 4c, for the sample annealed on the glass substrate, only a diffused diffraction ring is acquired, indicating that the preferred growth directions of PCBM crystals are completely random.

To shed light on the unique crystallization behavior of PCBM on mica, we have to understand the characteristic surface of freshly cleaved mica, in particular its lattice spacing in the plane exposed. Although it is well documented that many organic or inorganic crystals adopt epitaxial crystallization on the mica surface for their well-matching lattice parameters to mica surface,[34,45,46] however, there are few reports on the growth of PCBM nanocrystals on any substrates, due mainly to its still not very clear crystal structure.[43,44] Typically, the cleavage of a mica sheet will result in exposure of crystallographic (001) plane of mica crystal,[34,47] which is correspondingly served as the new substrate surface. As shown in Figure 5, it gives a schematic illustration of the crystallographic (001) plane of mica where the representative oxygen atoms adopt hexagonal alignment with typical lattice spacing $a = 0.46$ nm. Upon placing PCBM molecules onto this array according to the typical unit dimension of PCBM crystal within the $a-b$ plane, it could be found that center of each fullerene cage is exactly located on an oxygen atom and surrounded by the outer six oxygen atoms with hexagonal arrangement, which generates very small mismatch ratio of 2.8% in crystallographic a-axis of PCBM crystal, although a somewhat large mismatch of 8.6% in b-axis is obtained. Consequently, we are able to come to the conclusion that the crystallization of PCBM on mica surface adopts this epitaxial relation; the preferred growth direction of obtained rod- or ricelike PCBM crystals will form −60° or 60° with each other, as has already been verified by SAED patterns (Figures 2e and 3a) and the FFT images from optical micrographs shown in Figures 3 and 4, respectively.

As shown in Figure 4a,b, the PCBM crystals obtained through epitaxial growth are both abundant in amount and very homogeneous in their dispersion within the whole composite films, particularly the size of these crystals is much smaller compared with those obtained on the PEDOT:PSS surface which is commonly used as anode layer in a PV device. The formation of such uniformed PCBM crystals could be attributed to two reasons. One is the epitaxy-assisted nucleation of PCBM on mica surface, which leads to the formation of abundant nuclei homogeneously dispersed in the composite film for crystals to grow up. Second, due to the already formed large numbers of PCBM nuclei, there is a competition between these nuclei to incorporate the PCBM molecules diffusing within the matrix for further crystal growth, resulting in limited width of crystals. For the composite films annealed on the other substrates, no epitaxy-assisted nucleation is allowed, and thus the number of nuclei generated is very limited. As a consequence, these nuclei have an opportunity to exhaust more PCBM molecules during thermal annealing and result in larger crystals. Therefore, this unique epitaxy relationship between PCBM crystal and lattice spacing of mica surface has already shown its potential application in constructing homogeneously distributed PCBM crystals with nanoscale dimension in composite films. As has already been stated, the morphology of each component in the photoactive layer of polymer solar cells plays a key role in determining the device performance. A close-to-ideal but experimentally realizable morphology for polymer/fullerene photovoltaic cells based on bulk-heterojunction conception, as suggested in Figure 6, could satisfy 2-fold criterions simultaneously for high-performance PV device, i.e. a maximized interface for efficient exciton dissociation via a nanoscale (preferably around 20 nm) phase segregation between conjugated polymer and fullerene in lateral dimension and continuous (preferably perpendicular alignment so as to achieve short) pathways for free charge carriers to be transported to the appropriate electrodes. Upon applying this novel method to try to create nanoscale PCBM crystals in the P3HT:PCBM (1:1, w/w) composite films, the above-mentioned morphology is approximately achieved.

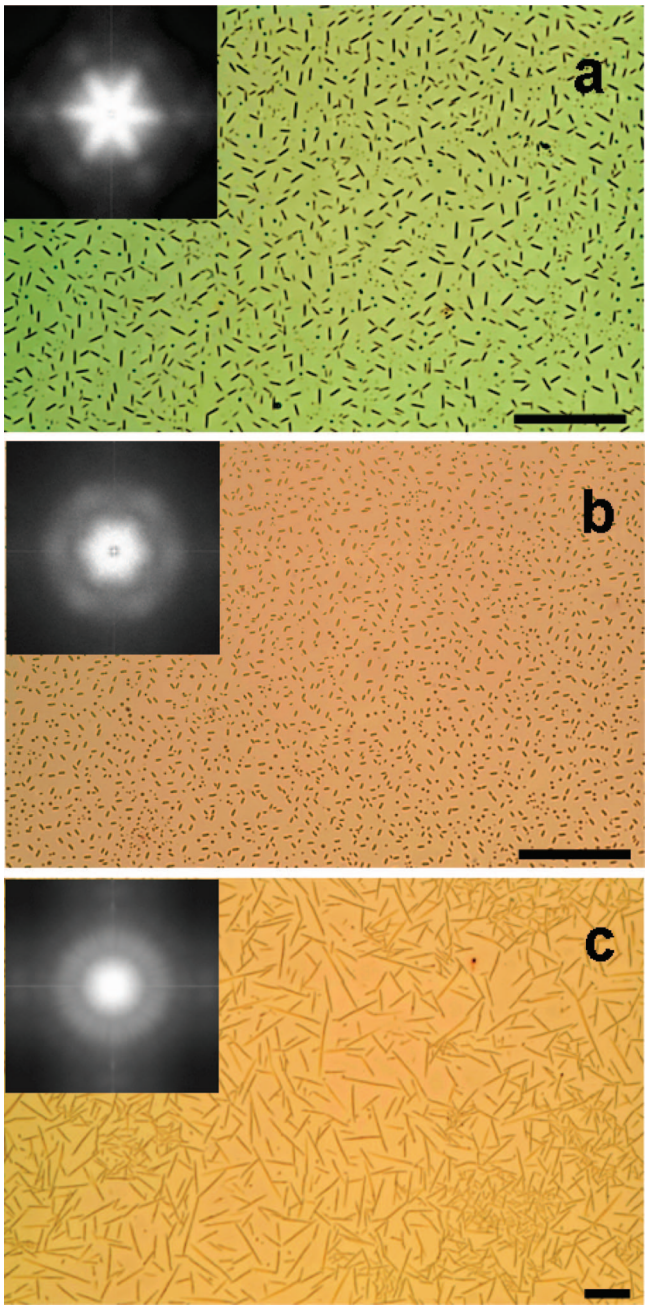

Figure 4. Optical microscopy images of PCBM crystals in different composite films after annealing at 150 °C for 30 min: (a) MDMO-PPV:PCBM (1:2, w/w) on mica; (b) P3HT:PCBM (1:1, w/w) on mica; (c) MDMO-PPV:PCBM (1:2, w/w) on glass. Inset in each image is its corresponding FFT pattern. Scale bar: 50 μm.

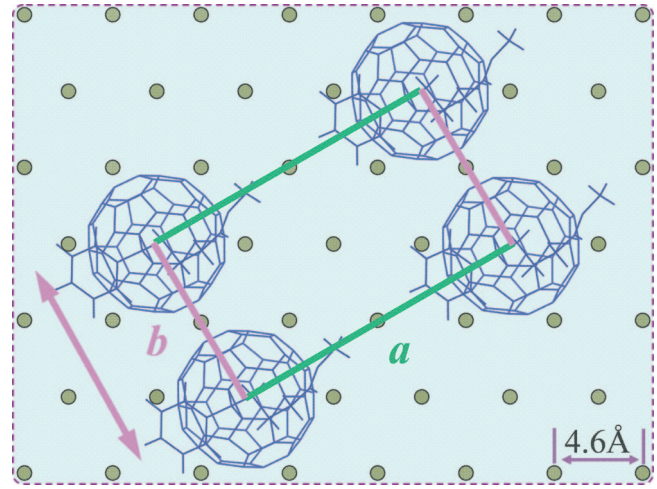

Figure 5. Schematic illustration demonstrating epitaxial growth of PCBM crystals on (001) lattice surface of freshly cleaved mica substrate.

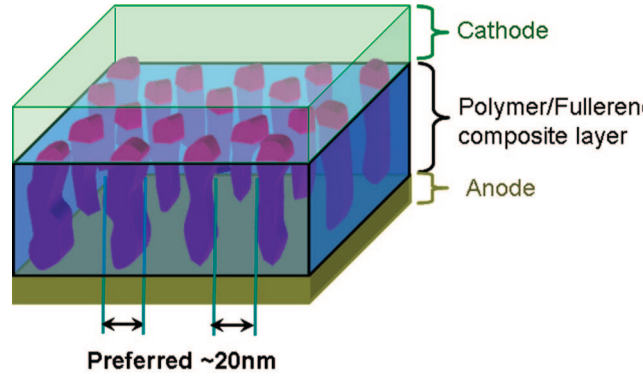

Figure 6. Schematic representation of a suggested close-to-ideal but experimentally realizable morphology for polymer/fullerene photovoltaic cells based on bulk-heterojunction conception.

However, for the real application in polymer solar cells, it would be expected that the size of PCBM crystals, particularly in lateral direction, could be further reduced so as to maximize interface area between the two components involved. It has been primarily verified that the temperature and time used for thermal annealing play an important role in determining the size and also the abundance of PCBM crystals in the composite film. Through adjusting these parameters, homogeneously dispersed PCBM nanocrystals with size of ca. 30 nm were created in the MDMO-PPV:PCBM (1:2, w/w) composite film, as shown in Figure 8a. In particular, the length scale of phase segregation is also in the order of 30 nm, which should be close-to-ideal morphology for BHJ-based polymer photovoltaic cells. With respect to the P3HT:PCBM (1:1, w/w) system (Figure 7b), homogeneously distributed PCBM nanocrystals with width of ca. 200 nm (shown by the width distribution in Figure 7c) could be achieved in the composite film upon annealing at 150 °C for 3 min on freshly cleaved mica surface. Nevertheless, when AFM measurement was performed on the gray area as shown by dashed blue circle in Figure 7b, close packed nanoparticles with a size of ca. 40 nm were found on the surface as shown in Figure 7d. We assigned them to PCBM nanocrystals for the reason that P3HT usually formed whiskerlike morphology in the thin films.[36] The amount of PCBM that is still mixed with P3HT in the matrix is estimated to be around 30% for this film. Consequently, the abundant PCBM nanocrystals created by epitaxy-assisted crystallization together with those close packed PCBM aggregates mixing with P3HT on the gray area contribute to the optimized morphology in which continuous pathways are constructed while large enough interfacial area is maintained for exciton dissociation. Nevertheless, it needs further delicate tailor on thermal annealing conditions, such as the annealing temperature, treatment time, confinement, etc., to achieve the further optimized morphology for the P3HT:PCBM composite system.

However, the most exciting expectation is still the feasibility and success of this novel method in the application of a real photovoltaic device which typically consists of a standard ITO/PEDOT:PSS/composite/LiF/Al architecture. Therefore, the composite film prepared via epitaxy-assisted crystallization method has to be removed from the original mica substrate and

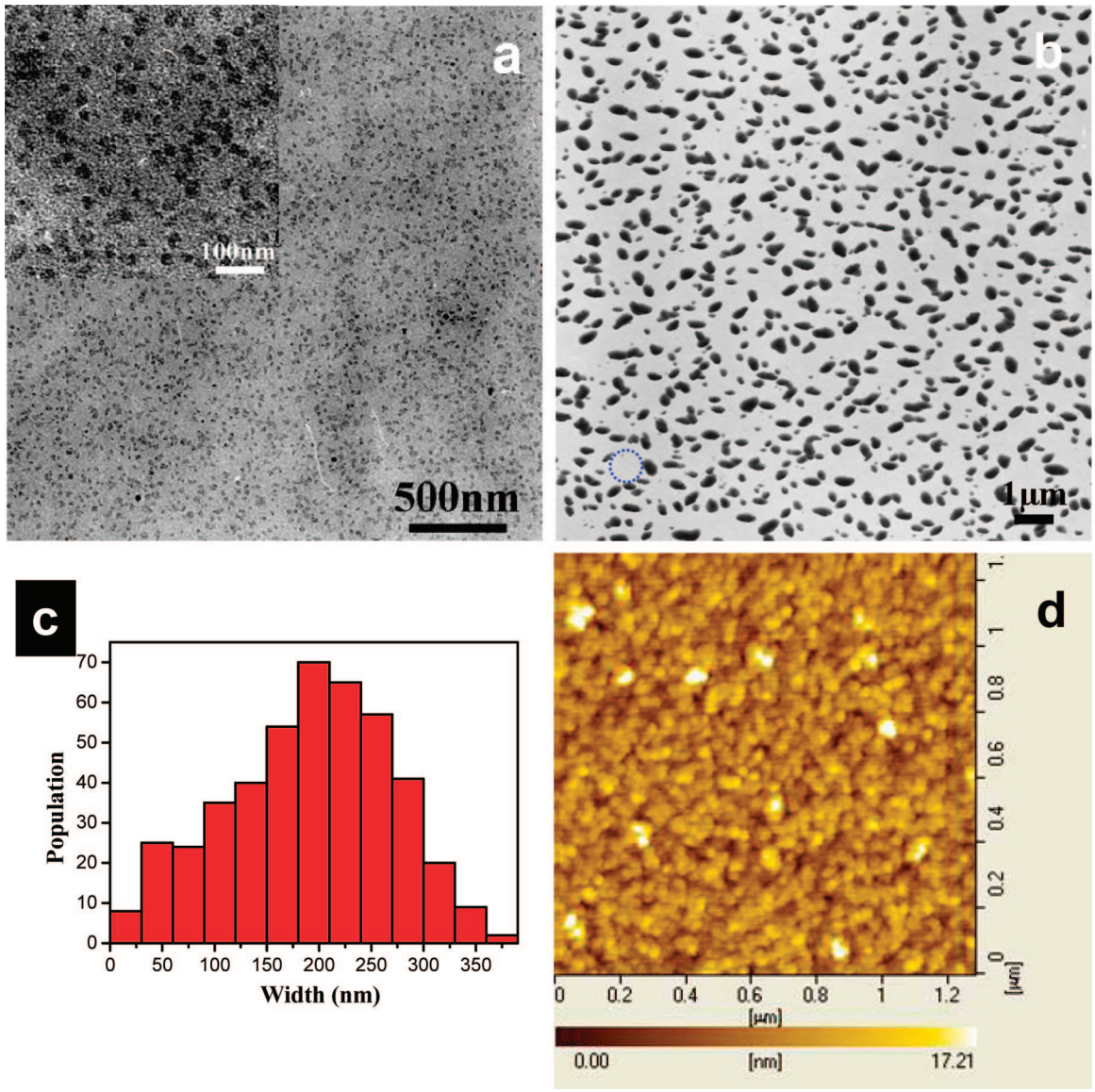

Figure 7. PCBM nanocrystals in MDMO-PPV:PCBM (1:2, w/w) (a) and P3HT:PCBM (1:1, w/w) films (b, c, d) after annealing on mica substrate: (a) 130 °C for 3 min, inset is the zoomed-in image of the same sample; (b) 150 °C for 3 min; (c) width distribution of PCBM nanocrystals in (b); (d) AFM topography image of the selected area in (b).

transferred onto a substrate with ITO/PEDOT:PSS layer, and then the device is completed with a top metal contact layer. As shown in Figure 8a, current density−voltage ($J-V$) measurements reveal that, for the device employed a thin P3HT:PCBM composite film having been annealed on mica substrate as the photoactive layer, short-circuit current density (J_{SC}) has been increased from 3.10 to 9.76 mA/cm^2, and also an increased fill factor (FF) from 0.34 to 0.40 has been achieved in contrast to the pristine device. Besides, though a somewhat decreased open-circuit voltage (V_{OC}) from 0.63 to 0.57 V is obtained, these parameters eventually still result in increased power conversion efficiency (PCE) from 0.66% for the pristine device to 2.23% for the device prepared via the novel method introduced in this work. After checking with optical absorption of photoactive layer between pristine film and the thermal annealed film on mica, as shown in Figure 8b, solely the increased absorption is far away enough to contribute to the more than 3 times increased current in the device. Therefore, the optimized morphology should be mainly responsible for this improvement; i.e., thermal annealing on mica creates homogenously distributed PCBM nanocrystals in the composite film. These PCBM nanocrystals penetrate through the whole film and contact directly with the cathode, which provide a shorter pathway for more efficient electron transportation to the cathode.

It should be noted that the overall efficiency of the PV device fabricated via this epitaxy approach is comparable to those cells prepared via post-thermal annealing or solvent vapor treatment, although it still needs to be further increased. However, the short-circuit current has reached a satisfied number, which implies the morphology of the composite film has already been substantially improved. Nevertheless, though more promising morphology is achieved in MDMO-PPV/PCBM composite, more dedicated efforts need to be paid to the MDMO-PPV/PCBM system for the chemistry instability of MDMO-PPV while exposing to oxygen or humidity, which usually results in substantial performance degradation. Anyhow, for the first time, we have successfully demonstrated a novel method to create PCBM nanocrystals and their homogeneous dispersion in the composite film for high-performance bulk-heterojunction polymer solar cells using epitaxy-assisted crystallization on mica surface. The feasibility of this method has been successfully proven by the substantially improved device performance. As

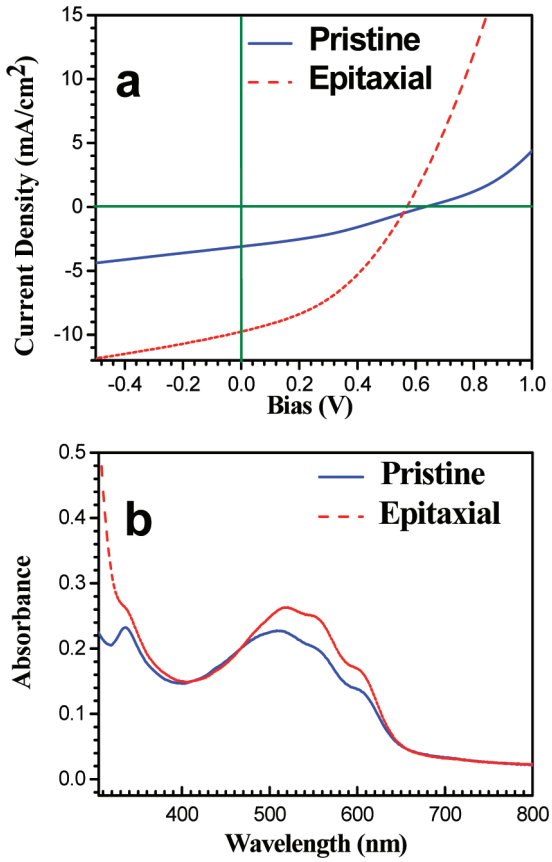

Figure 8. (a) Current density−voltage characteristics of P3HT:PCBM (1:1, by weight) devices transferred from mica substrates and (b) corresponding UV−vis absorbance spectra. Blue solid line: pristine device; red dashed line: the epitaxy treated device via annealing at 150 °C for 3 min on mica.

we have known, although the crystallizability of PCBM has been reduced after chemical decoration on the cage compared with its original form fullerene C_{60}, it still crystallizes easily. Correspondingly, morphology control for this component in the composite toward specific requirements needs more tricks. Otherwise, one frequently faces the situations with either almost molecularly distributed PCBM in the polymer matrix, which prevents electron transportation to the cathode, or a composite with large-scale phase separation composed of PCBM crystals with the size of several microns, which has not enough interface for efficient exciton dissociation. However, the novel method we demonstrated here could create PCBM nanocrystals with abundant population, homogeneous dispersion, and controllable size for high-performance polymer solar cells. Therefore, we have actually demonstrated a new approach to construct the desired morphology for high-performance optoelectronic devices via resorting to other specific substrate which could induce formation of this type of morphology.

Conclusions

In summary, we have demonstrated a novel method to create nanoscale PCBM crystals homogeneously dispersed in the composite film of conjugated polymer, e.g. MDMO-PPV and P3HT for high-performance polymer solar cells using epitaxy assisted crystallization. As revealed by TEM micrographs, SAED patterns, OM images, and the quantitative analysis by using FFT, PCBM could carry out epitaxial growth on freshly cleaved mica where unit cell parameters of PCBM crystal well match with crystallographic (001) lattice plane of mica crystal. This epitaxy relationship results in a large number of PCBM nuclei upon thermal annealing on the mica substrate, which subsequently develop into PCBM nanocrystals with homogeneous dispersion in the composite film. The hexagonal lattice of the substrate induces formation of PCBM crystals taking an angle of either −60° or 60° with each other. The feasibility of this novel method in the real PV device fabrication has been proven by substantially enhanced device performance, in particular the improvement of short circuit current, which is heavily dependent on the morphology of the photoactive layer. Although further optimization has to be taken into consideration so as this method could fully benefit the device performance, we have shown a novel approach to construct an optimized morphology for polymer solar cells based on fullerene composite and its experimental feasibility. We further note the application of this epitaxy-assisted crystal growth is not confined to the polymer photovoltaic cells but could also be extended to other devices so as to control the morphology on their crystallizable components.

Acknowledgment. This work was financially supported by National Natural Science Foundation of China (Grant No. 20604029, 20874100). X.N.Y. thanks the supports from the Fund for Creative Research Groups (Grant No. 50621302).

References and Notes

(1) Brabec, C. J.; Sariciftci, N. S.; Hummelen, J. C.; Padinger, F.; Fromherz, T.; Hummelen, J. C. *Adv. Funct. Mater.* **2001**, *11*, 15.
(2) Hoppe, H.; Sariciftci, N. S. *J. Mater. Res.* **2004**, *19*, 1924.
(3) Coakley, K. M.; McGehee, M. D. *Chem. Mater.* **2004**, *16*, 4533.
(4) Campos, L. M.; Tontcheva, A.; Günes, S.; Sonmez, G.; Neugebauer, H.; Sariciftci, N. S.; Wudl, F. *Chem. Mater.* **2005**, *17*, 4031.
(5) Wienk, M. M.; Kroon, J. M.; Verhees, W. J. H.; Knol, J.; Hummelen, J. C.; Hal, P. A. v.; Janssen, R. A. J. *Angew. Chem., Int. Ed.* **2003**, *42*, 3371.
(6) Mühlbacher, D.; Scharber, M.; Morana, M.; Zhu, Z.; Waller, D.; Gaudiana, R.; Brabec, C. *Adv. Mater.* **2006**, *18*, 2884.
(7) Yang, X. N.; Loos, J.; Veenstra, S. C.; Verhees, W. J. H.; Wienk, M. M.; Kroon, J. M.; Michels, M. A. J.; Janssen, R. A. J. *Nano Lett.* **2005**, *5*, 579.
(8) Yang, X. N.; Lu, G. H.; Li, L. G.; Zhou, E. L. *Small* **2007**, *3*, 611.
(9) Shaheen, S. E.; Brabec, C. J.; Sariciftci, N. S. *Appl. Phys. Lett.* **2001**, *78*, 841.
(10) Hoppe, H.; Sariciftci, N. S. *J. Mater. Chem.* **2006**, *16*, 45.
(11) Yang, C.; Hu, J. G.; Heeger, A. J. *J. Am. Chem. Soc.* **2006**, *128*, 12007.
(12) Yang, F.; Sun, K.; Forrest, S. R. *Adv. Mater.* **2007**, *19*, 4166.
(13) Yang, X. N.; Joachim, L. *Macromolecules* **2007**, *40*, 1353.
(14) Li, L. G.; Lu, G. H.; Yang, X. N. *J. Mater. Chem.* **2008**, *18*, 1984.
(15) Lee, J. K.; Ma, W. L.; Brabec, C. J.; Yuen, J.; Moon, J. S.; Kim, J. Y.; Lee, K.; Bazan, G. C.; Heeger, A. J. *J. Am. Chem. Soc.* **2008**, *130*, 3619.
(16) Wienk, M. M.; Turbiez, M.; Gilot, J.; Janssen, R. A. J. *Adv. Mater.* **2008**, *20*, 2556.
(17) Berson, S.; Bettignies, R. D.; Bailly, S.; Guillerez, S. *Adv. Funct. Mater.* **2007**, *17*, 1377.
(18) Yu, G.; Gao, J.; Hummelen, J. C.; Wudl, F.; Heeger, A. J. *Science* **1995**, *270*, 1789.
(19) Ganesan, P.; Yang, X. N.; Loos, J.; Savenije, T. J.; Abellon, R. D.; Zuilhof, H.; Sudholter, E. J. R. *J. Am. Chem. Soc.* **2005**, *127*, 14530.
(20) Sivula, K.; Luscombe, C. K.; Thompson, B. C.; Fréchet, J. M. J. *J. Am. Chem. Soc.* **2006**, *128*, 13988.
(21) Yang, X. N.; Alexeev, A.; Michels, M. A. J.; Loos, J. *Macromolecules* **2005**, *38*, 4289.
(22) Kietzke, T.; Neher, D.; Kumke, M.; Montenegro, R.; Landfester, K.; Scherf, U. *Macromolecules* **2004**, *37*, 4882.
(23) Gur, I.; Fromer, N. A.; Chen, C.-P.; Kanaras, A. G.; Alivisatos, A. P. *Nano Lett.* **2007**, *7*, 409.
(24) Lu, G. H.; Li, L. G.; Yang, X. N. *Small* **2008**, *4*, 601.
(25) Padinger, F.; Rittberger, R. S.; Sariciftci, N. S. *Adv. Funct. Mater.* **2003**, *13*, 85.
(26) Li, G.; Shrotriya, V.; Huang, J.; Yao, Y.; Moriarty, T.; Emery, K.; Yang, Y. *Nat. Mater.* **2005**, *4*, 864.
(27) Zhao, Y.; Xie, Z.; Qu, Y.; Geng, Y.; Wang, L. *Appl. Phys. Lett.* **2007**, *90*, 043504.

(28) Li, G.; Yao, Y.; Yang, H.; Shrotriya, V.; Yang, G.; Yang, Y. *Adv. Funct. Mater.* **2007**, *17*, 1636.

(29) Swinnen, A.; Haeldermans, I.; Ven, M. v.; D'Haen, J.; Vanhoyland, G.; Aresu, S.; D'Olieslaeger, M.; Manca, J. *Adv. Funct. Mater.* **2006**, *16*, 760.

(30) Ma, W. L.; Yang, C. Y.; Gong, X.; Lee, K.; Heeger, A. J. *Adv. Funct. Mater.* **2005**, *15*, 1617.

(31) Peet, J.; Kim, J. Y.; Coates, N. E.; Ma, W. L.; Moses, D.; Heeger, A. J.; Bazan, G. C. *Nat. Mater.* **2007**, *6*, 497.

(32) Kim, J. Y.; Lee, K.; Coates, N. E.; Moses, D.; Nguyen, T.-Q.; Dante, M.; Heeger, A. J. *Science* **2007**, *317*, 222.

(33) Otero, R.; Ecija, D.; Fernández, G.; Gallego, J. M.; Sánchez, L.; Martín, N.; Miranda, R. *Nano Lett.* **2007**, *7*, 2602.

(34) Plank, H.; Resel, R.; Purger, S.; Keckes, J.; Thierry, A.; Lotz, B.; reev, A.; Sariciftci, N. S.; Sitter, H. *Phys. Rev. B* **2001**, *64*, 235423.

(35) Brinkmann, M.; Wittmann, J.-C. *Adv. Mater.* **2006**, *18*, 860.

(36) Ihn, K. J.; Moulton, J.; Smith, P. *J. Polym. Sci., Part B: Polym. Phys.* **1993**, *31*, 735.

(37) Rosa, C. D.; Park, C.; Lotz, B.; Wittmann, J.-C.; Fetters, L. J.; Thomas, E. L. *Macromolecules* **2000**, *33*, 4871.

(38) Mitchell, C. A.; Yu, L.; Ward, M. D. *J. Am. Chem. Soc.* **2001**, *123*, 10830.

(39) Moggio, I.; Moigne, J. L.; Arias-Marin, E.; Issautier, D.; Thierry, A.; Comoretto, D.; Dellepiane, G.; Cuniberti, C. *Macromolecules* **2001**, *34*, 7091.

(40) Yang, X. N.; van Duren, J. K. J.; Janssen, R. A. J.; Michels, M. A. J.; Loos, J. *Macromolecules* **2004**, *37*, 2151.

(41) Yang, X. N.; van Duren, J. K. J.; Rispens, M. T.; Hummelen, J. C.; Janssen, R. A. J.; Michels, M. A. J.; Loos, J. *Adv. Mater.* **2004**, *16*, 802.

(42) Rispens, M. T.; Meetsma, A.; Rittberger, R.; Brabec, C. J.; Sariciftci, N. S.; Hummelen, J. C. *Chem. Commun.* **2003**, 2116.

(43) Écija, D.; Otero, R.; Sánchez, L.; Gallego, J. M.; Wang, Y.; Alcamí, M.; Martín, F.; Martín, N.; Miranda, R. *Angew. Chem., Int. Ed.* **2007**, *46*, 7874.

(44) Wang, Y.; Alcamí, M.; Martín, F. *ChemPhysChem.* **2008**, *9*, 1030.

(45) Zhang, X. W.; Chen, N. F.; Yan, F.; Goedel, W. A. *Appl. Phys. Lett.* **2005**, *86*, 203102.

(46) Josefowicz, J. Y.; Avlyanov, J. K.; MacDiarmid, A. G. *Thin Solid Films* **2001**, *393*, 186.

(47) Plank, H.; Resel, R.; Andreev, A.; Sariciftci, N. S.; Sitter, H. *J. Cryst. Growth* **2002**, *237−239*, 2076.

JP8081529